© 2015. Published by The Company of Biologists Ltd | Development (2015) 142, 2888-2893 doi:10.1242/dev.120212

RESEARCH REPORT

STEM CELLS AND REGENERATION

Retinoic acid signaling spatially restricts osteoblasts and controls ray-interray organization during zebrafish fin regeneration

Nicola Blum[1,2] and Gerrit Begemann[1,*]

ABSTRACT

The zebrafish caudal fin consists of repeated units of bony rays separated by soft interray tissue, an organization that must be faithfully re-established during fin regeneration. How and why regenerating rays respect ray-interray boundaries, thus extending only the existing bone, has remained unresolved. Here, we demonstrate that a retinoic acid (RA)-degrading niche is established by Cyp26a1 in the proximal basal epidermal layer that orchestrates ray-interray organization by spatially restricting osteoblasts. Disruption of this niche causes preosteoblasts to ignore ray-interray boundaries and to invade neighboring interrays where they form ectopic bone. Concomitantly, non-osteoblastic blastema cells and regenerating blood vessels spread into the interrays, resulting in overall disruption of ray-interray organization and irreversible inhibition of fin regeneration. The *cyp26a1*-expressing niche plays another important role during subsequent regenerative outgrowth, where it facilitates the Shha-promoted proliferation of osteoblasts. Finally, we show that the previously observed distal shift of ray bifurcations in regenerating fins upon RA treatment or amputation close to the bifurcation can be explained by inappropriate preosteoblast alignment and does not necessarily require putative changes in proximodistal information. Our findings uncover a mechanism regulating preosteoblast alignment and maintenance of ray-interray boundaries during fin regeneration.

KEY WORDS: Cyp26a1, Caudal fin, Zebrafish, Regeneration, Osteoblast, Interray

INTRODUCTION

Zebrafish regenerate amputated fins by establishing lineage-restricted blastema cells (Gemberling et al., 2013; Tanaka and Reddien, 2011). The zebrafish caudal fin possesses 16-18 fin rays, each consisting of two segmented and opposing hemirays of acellular bone that surround a core of fibroblasts, osteoblasts, pigment cells, arterial blood vessels and nerves (Fig. 1A) (Akimenko et al., 2003). Fin rays are separated by boneless interray tissue, composed of fibroblasts, venous blood vessels, pigment cells and nerves. The principles that compel regenerating fin rays to respect ray-interray boundaries, therefore confining regenerating bone to extend the existing rays, are still unknown. Upon fin amputation, osteoblasts that cover the hemiray surfaces dedifferentiate into proliferating preosteoblasts and migrate into the nascent blastema, where they align at proximal lateral positions (Knopf et al., 2011; Sousa et al., 2011; Stewart and Stankunas, 2012). Thus, preosteoblasts form a layer between the basal epidermal layer and fibroblast-derived blastema cells. The distal blastema remains devoid of preosteoblasts. During subsequent regenerative outgrowth, proliferating preosteoblasts at the distal leading edge become differentiating osteoblasts in more proximal parts (Stewart et al., 2014). Notably, neither osteoblasts nor non-osteoblastic blastema cells mix with adjacent interray cells (Stewart and Stankunas, 2012). Thus, the regenerating fin consists of repeating blastema units dedicated to each fin ray that are separated by regenerating interrays (Fig. 1A).

[1]Developmental Biology, University of Bayreuth, Bayreuth 95440, Germany. [2]RTG1331, Department of Biology, University of Konstanz, Konstanz 78457, Germany.

*Author for correspondence (gerrit.begemann@uni-bayreuth.de)

Received 23 November 2014; Accepted 22 July 2015

RESULTS AND DISCUSSION

cyp26a1-expressing epidermal niches control preosteoblast alignment and ray-interray organization

During fin regeneration, fin rays respect ray-interray boundaries. An interesting exception occurs after amputation close to a bifurcation site (short cut, Fig. 1B). In such regenerates, sister rays ignore ray-interray boundaries and fuse (Fig. 1C) (Laforest et al., 1998), whereby the probability for ray fusion increases as the distance between them decreases (Fig. 1D). Using the *osc:gfp* line, which allows detection of preosteoblasts in the early blastema (Knopf et al., 2011; Sousa et al., 2011), we found ectopic preosteoblasts in the interray separating the two sister rays at 2 dpa (Fig. 1E). This finding reveals that sister ray fusion is due to preosteoblasts spreading into the interray. We were interested in the mechanisms that cause preosteoblasts to respect ray-interray boundaries. *shha* is expressed within the basal epidermal layer adjacent to pre- and differentiating osteoblasts (supplementary material Fig. S1) (Laforest et al., 1998; Lee et al., 2009; Quint et al., 2002; Zhang et al., 2012). We found a similar expression pattern for the RA-degrading enzyme *cyp26a1* (Fig. 1F,G). By contrast, the RA-synthesizing enzyme *aldh1a2* is expressed in fibroblast-derived blastema cells (Fig. 1G) (Blum and Begemann, 2012). Although proximal fibroblast-derived blastema cells express *cyp26b1* (Blum and Begemann, 2015), it is unlikely that RA diffusion into adjacent epidermal cells is efficiently prevented. We thus suspected that *cyp26a1*-expressing cells provide niches of low RA levels that might facilitate expression of RA-sensitive genes.

It has been shown that immersion of fish in RA reduces *shha* expression (Laforest et al., 1998). However, RA administration via immersion induces epidermal cell death (Ferretti and Géraudie, 1995; Géraudie and Ferretti, 1997); therefore, it has remained unclear whether this was a specific effect. We used intraperitoneal (IP) injection of RA, which efficiently enhances RA levels in the adult fin without causing cell death (Blum and Begemann, 2012), and found decreased expression of *shha* and of the Hh receptor and target *ptch2* 6 h after injection at 4 dpa (Fig. 1H). Injection of R115866, a selective antagonist of Cyp26 enzymes (Hernandez et al., 2007; Stoppie et al., 2000), also caused downregulation of *shha* and *ptch2* (Fig. 1H,I), indicating that *shha* expression requires RA degradation. Accordingly, overexpression of *cyp26a1* in *hsp70l:*

Development (2015) 142, 2888-2893 doi:10.1242/dev.120212

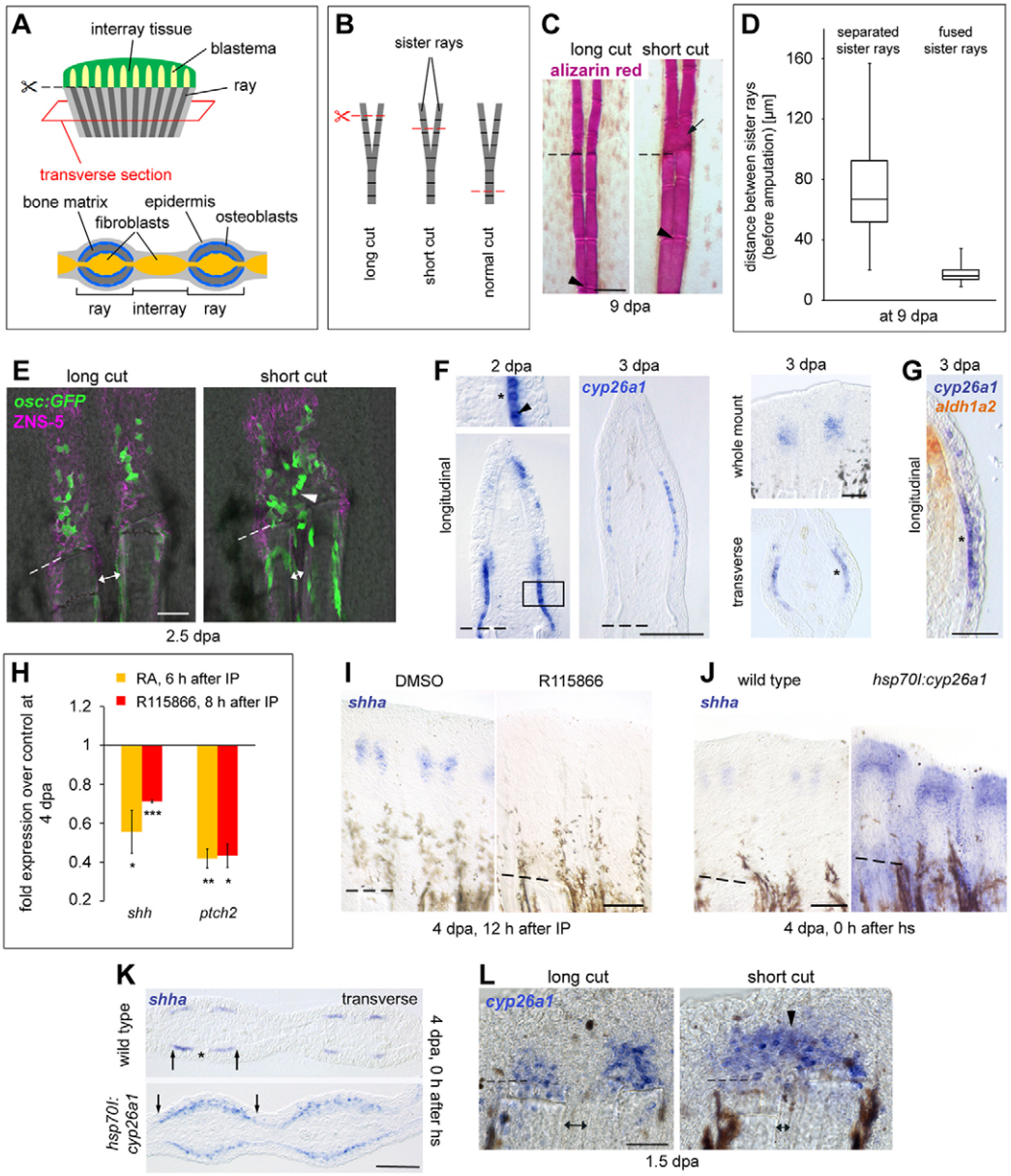

Fig. 1. *shha* expression is controlled by *cyp26a1*-expressing epidermal niches. Lateral expansion of the *cyp26a1*-expressing niches and misguidance of preosteoblasts precede fusion of sister rays. (A) Overview of a regenerating fin. (B) Schematized representation of the amputation levels. (C-E,L) Amputations in proximity to bifurcations cause fusion of *cyp26a1* expression domains (arrowhead in L), followed by spreading of preosteoblasts into the interray separating the two sister rays (arrowhead in E) and fusion of sister rays (arrow in C). (C) Alizarin Red staining at 9 dpa. Arrowheads indicate branching sites. (D) Distance range between sister rays for separated and fused rays. (E) IHC for ZNS-5 and GFP in *osc:gfp* fish at 2.5 dpa. (F,G) WISH and ISH on sections for *cyp26a1* reveals expression in the proximal basal epidermal layer (arrowhead) adjacent to preosteoblasts (asterisks) at 2 and 3 dpa. (G) *aldh1a2* is expressed in fibroblast-derived blastema cells, but not in preosteoblasts adjacent to *cyp26a1*-expressing cells. (H,I) RA and R115866 injection downregulates *shha* and *ptch2*. Transcript levels 6 or 8 hours after injection at 4 dpa measured by qPCR (H); WISH for *shha* 12 hours after R115866 injection at 4 dpa (I). (J,K) Overexpression of *cyp26a1* in *hsp70l:cyp26a1* fish at 4 dpa causes upregulation of *shha* expression and lateral expansion of the expression domains. Arrows mark the lateral expression limits. Of note, *shha* in wild-type controls is already expressed in subdomains due to the upcoming bifurcation event. (L) WISH for *cyp26a1* at 1.5 dpa. Double-headed arrows in E and L: distance between sister rays. Asterisk marks the gap between the two subdomains. Data are represented as mean±s.e.m. **P*<0.05, ***P*<0.01, ****P*<0.001. Dashed lines indicate amputation plane. Scale bars: 100 µm. h, hours; hs, heat shock.

cyp26a1 fish (Blum and Begemann, 2012) at 4 dpa resulted in enhanced and laterally extended *shha* expression within the basal epidermal layer directly at the end of a single heat shock (Fig. 1J,K). We did not observe *shha* expression in interrays. We propose that this was due to the requirement for Fgfs (and putative other blastema-derived signals) for *shha* expression (Lee et al., 2009).

Short-cut amputations resulted in shared *cyp26a1* expression domains between sister rays at 1.5 dpa (Fig. 1L), indicating that fusion of the RA-degrading niches precedes spreading of preosteoblasts into interrays. To examine how preosteoblasts behave if efficient lowering of RA levels in the *cyp26a1*-niches fails, we injected fish with RA or R115866, starting with the first IP directly after amputation (normal cut). We observed spreading of preosteoblasts into interrays in RA- and R115866-injected *osc:gfp* fish at 2.5 dpa (Fig. 2A; data not shown), indicating that preosteoblasts failed to align at proximolateral parts of the

Development (2015) 142, 2888-2893 doi:10.1242/dev.120212

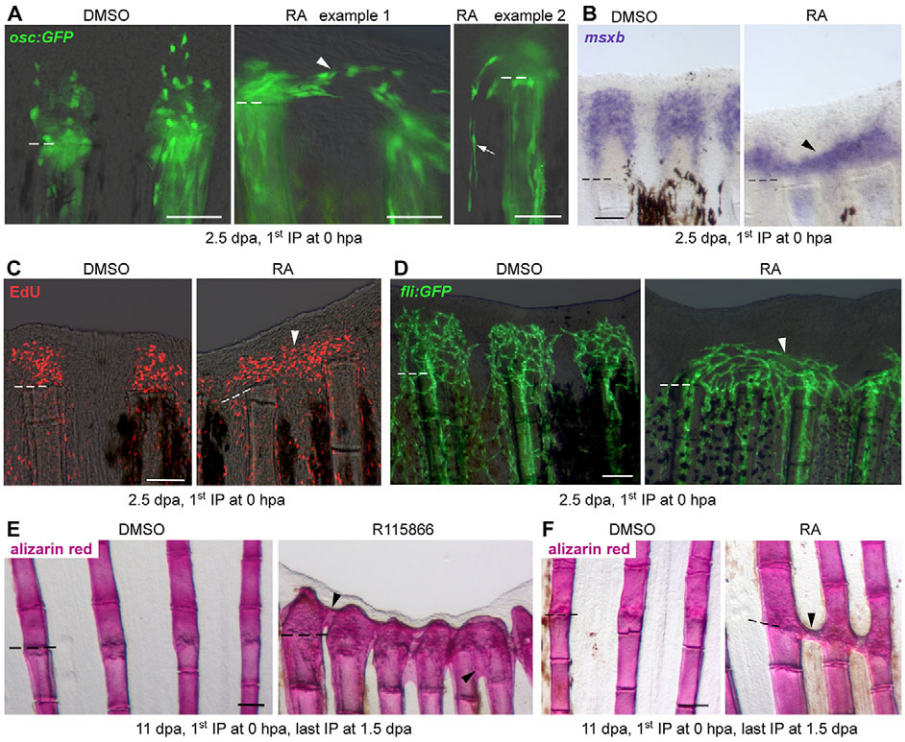

Fig. 2. Preosteoblast alignment and maintenance of the ray-interray organization requires RA-degrading epidermal niches. (A) IHC for GFP in *osc:gfp* fish reveals ectopic GFP$^+$ preosteoblasts in interrays in RA-treated fish at 2.5 dpa. Arrowhead indicates preosteoblast in interray tissue, arrow indicates proximally migrating preosteoblast in interray tissue. (B,C) WISH for *msxb* (B) and EdU labeling (C) at 2.5 dpa demonstrate expansion of blastema cells into interrays in RA-treated fish. Arrowheads indicate ectopic blastema cells. (D) *fli:gfp* fish show misconnected blood vessels (arrowhead) in RA-treated fish at 2.5 dpa. (E,F) RA and R115866 treatment during blastema formation result in formation of ectopic bone at the wound site and in R115866-treated fish in an irreversible regeneration block. Arrowheads indicate ectopic bone, dashed lines indicate amputation plane. Scale bars: 100 µm.

blastema and disregarded ray-interray boundaries. Of note, formation of a distinct basal epidermal layer was not inhibited (supplementary material Fig. S2A). As R115866 treatment also reduced Cyp26b1 activity in fibroblast-derived blastema cells, we cannot exclude that misguidance of preosteoblasts in R115866- or RA-treated fish was at least partially due to enhanced RA levels in the mesenchyme. However, the expression pattern of *cyp26a1* strongly supports a model in which alignment, and thereby spatial restriction of preosteoblasts, is controlled by signals from *cyp26a1*-expressing epidermal cells.

Interestingly, treatment with RA or R115866 also caused expansion of the blastema marker *msxb* (Akimenko et al., 1995) into interrays (Fig. 2B; supplementary material Fig. S2B). 5-ethynyl-2′-deoxyuridine (EdU) labeling further suggested that these were cycling blastema cells (Fig. 2C). We did not observe an enlarged preosteoblast or *msxb*$^+$ cell population in RA- or R115866-treated fish (Fig. 2A,B; supplementary material Fig. S2B), thus making it unlikely that spreading into interrays was simply due to increased cell numbers.

Blood vessels regenerate into the blastema accompanied by anastomosis between the injured arteries and veins of the same ray (Huang et al., 2003). Intriguingly, wounded arteries and veins had formed connections with vessels of neighboring rays in RA- and R115866-treated *fli:gfp* fish (Lawson and Weinstein, 2002) at 2.5 dpa (Fig. 2D; data not shown). Together, these data show that also non-osteoblastic cell types ignore ray-interray boundaries if efficient RA degradation in the proximal basal epidermal layer fails.

Expansion of *msxb* expression into interrays was also observed in regenerates that lacked preosteoblasts, but showed expression of *cyp26a1* (supplementary material Fig. S3). This was achieved by treating fish with the Hh inhibitor cyclopamine from 24 hpa onwards, a treatment condition that is expected to inhibit preosteoblast proliferation in the stump. We thus conclude that, rather than signals from *cyp26a1*-expressing cells, aligning preosteoblasts themselves provide spatial orientation for non-osteoblastic blastema cells.

To test how disrespect of ray-interray boundaries by blastema cells affects the overall organization of the regenerating fin, we gave the last RA or R115866 injection at 1.5 dpa and examined the long-term consequences for regeneration. Of note, owing to autoregulatory feedback mechanisms of RA signaling, *cyp26a1* expression became upregulated in the entire regenerate during RA or R115866 treatment (data not shown). This upregulation can only counterbalance small fluctuations in RA levels and can therefore be neglected during the treatment period. However, ectopic expression persisted for some days after termination of treatment (supplementary material Fig. S4A), and was therefore expected to allow for *shha* expression in the entire regenerate. Consistently, we detected *shha* expression in both rays and interrays in R115866-treated *shh:gfp* fish (Ertzer et al., 2007) 2 days after treatment was stopped at 4 dpa (supplementary data Fig. S4B). As heat shock-induced overexpression of *cyp26a1* at 4 dpa is insufficient to induce *shha* expression in interrays (Fig. 1J,K), this result suggests that *shha* expression in interrays in R115866-treated fish was due to ectopic blastema cells in the interray region. Thus, this finding supports a model in which *shha* expression is spatially confined by RA-degrading epidermal cells and signals from underlying blastema cells.

In fins of R115866-treated fish, regeneration was subsequently irreversibly blocked and ectopic bone had formed in interrays at 11 dpa (Fig. 2E). However, bone matrix did not seal the wound (supplementary material Fig. S5), indicating that inhibition of regeneration was not due to a mechanical block but rather due to mispatterning of the early regenerate. In RA-treated fins, neighboring rays were occasionally connected by bony bridges at the amputation site (Fig. 2F), but otherwise, regeneration proceeded normally. This weaker phenotype was probably due to rapid clearance of excess RA after treatment had stopped. When fins were amputated within the third segment distal to the first branching point (long cut), RA treatment caused fusions of sister rays (supplementary material Fig. S6A). This is consistent with results

Development (2015) 142, 2888-2893 doi:10.1242/dev.120212

obtained previously by RA treatment via immersion (Géraudie and Ferretti, 1997; Géraudie et al., 1995; White et al., 1994). We next determined the distance range at which formation of ectopic bone occurs, and found a much greater range in RA-treated fish (supplementary material Fig. S6B). Fusion of sister rays had sometimes been interpreted as a proximalization of the regenerate (White et al., 1994). However, our data show that sister rays fuse if preosteoblasts spread into interrays, which can be caused either by insufficient lowering of RA levels in the proximal basal epidermal layer or by induction of two RA-degrading domains in close proximity. Thus, our findings provide a more parsimonious explanation for sister ray fusion that is not based on putative changes in proximodistal information.

Cyp26a1 activity facilitates osteoblast proliferation through *shha* expression

Proliferation of preosteoblasts has been suggested to be controlled by Shha (Laforest et al., 1998; Lee et al., 2009; Quint et al., 2002; Zhang et al., 2012). We found reduced osteoblast proliferation within 12 h of cyclopamine treatment (Fig. 3A). Osteoblast differentiation was unaffected (supplementary data Fig. S7). Moreover, we did not detect TUNEL^{+} osteoblasts in control or cyclopamine-treated fish (data not shown). Hence, even though RA signaling promotes osteoblast proliferation (Blum and Begemann, 2015), prolonged experimental RA exposure should cause downregulation of *shha* and consequently lead to a reduction of osteoblast proliferation. Indeed, osteoblast proliferation was reduced 12 h after RA injection at 3 dpa (Fig. 3B). Neither osteoblasts nor other cells undergo cell death after RA treatment via IP injections (Blum and Begemann, 2012). Concomitant activation of Hh signaling, using the Smoothened agonist SAG, rescued osteoblast proliferation (Fig. 3C), thus confirming that decreased proliferation upon RA treatment was due to impaired Hh signaling. Together, these findings indicate that Shha from *cyp26a1*-expressing epidermal cells promotes proliferation of adjacent osteoblasts. Interestingly, cyclopamine treatment has been reported to block proliferation of fibroblast-derived blastema cells (Lee et al., 2009), for which *ptch* expression has not been demonstrated. Accordingly, prolonged RA treatment downregulated proliferation of fibroblast-derived blastema cells, and concomitant SAG treatment could rescue this effect (supplementary material Fig. S8). Although we cannot exclude a direct effect, Hh signaling might indirectly promote proliferation of other cell types via osteoblasts.

Besides a requirement for *shha* expression, Fgf signaling has been shown to exclude *shha* from distal regions (Lee et al., 2009), suggesting that Fgf signaling restricts *shha* to the proximal basal epidermal layer by repressing *cyp26a1*. We manipulated Fgf signaling at 3 dpa by either overexpressing a dominant negative Fgfr1 (*hsp70l:dn-fgfr1*; Lee et al., 2005) or a constitutively active Ras (*hsp70l:v-ras*; Lee et al., 2009) and quantified *cyp26a1* expression. *cyp26a1* was downregulated in *hsp70l:v-ras* fish 2 h after a single heat shock and upregulated in *hsp70l:dn-fgfr1* fish at the end of a single heat shock (Fig. 3D), demonstrating that Fgf signaling inhibits *cyp26a1* expression. Thus, proximal expansion of Fgf signaling should result in proximal regression of *cyp26a1* expression. We took advantage of the finding that Fgf activity expands more proximally in fins that had been amputated at a more proximal position and retracts distally as regeneration proceeds

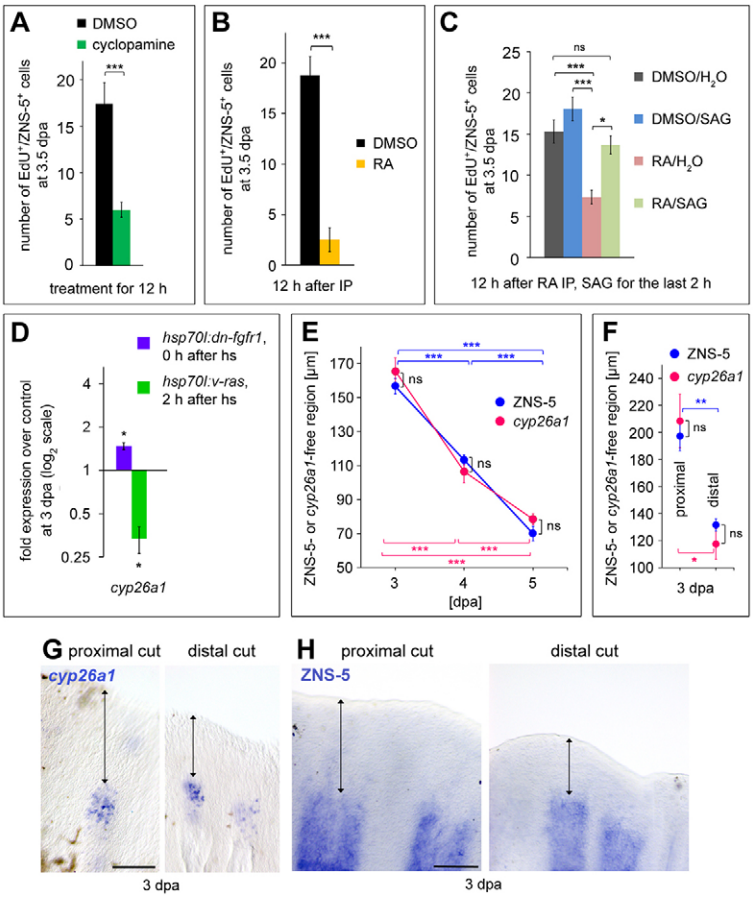

Fig. 3. Shha-promoted osteoblast proliferation requires *cyp26a1* expression that is restricted to proximal regions by Fgf activity. (A,B) Cyclopamine (A) or prolonged RA (B) treatment downregulates osteoblast proliferation. EdU^{+}/ZNS-5^{+} cells per section at 3.5 dpa. (C) Inhibition of osteoblast proliferation 12 h after RA injection can be rescued by concomitant SAG treatment. EdU^{+}/ZNS-5^{+} cells per section at 3.5 dpa. (D) Inhibition of Fgf signaling in *hsp70l:dn-fgfr1* fish results in upregulation of *cyp26a1* expression. Conversely, activation of Fgf signaling in *hsp70l:v-ras* fish results in the downregulation of *cyp26a1*. Transcript levels at 3 dpa measured by qPCR. (E-H) ZNS-5- and *cyp26a1*-free distal domains (double-headed arrows) extend further proximally in regenerates that had been amputated at a more proximal level at 3 dpa (F-H), and retracts distally as regeneration proceeds (E). (G) WISH for *cyp26a1*. (H) IHC for ZNS-5. (E,F) Length of the *cyp26a1*- or ZNS-5-free distal domain. Data are represented as mean±s.e.m. **P*<0.05, ***P*<0.01, ****P*<0.001. ns, not significant; hs, heat shock. Scale bars: 100 µm.

Development (2015) 142, 2888-2893 doi:10.1242/dev.120212

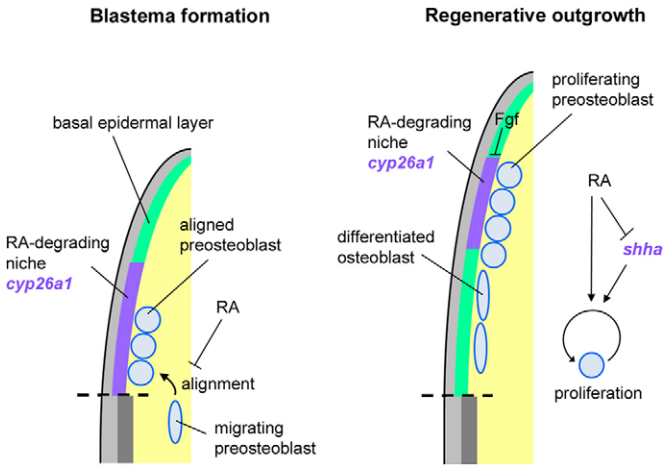

Fig. 4. Model for Cyp26a1 functions during fin regeneration. Schematic summary of Cyp26a1-mediated preosteoblast alignment and proliferation.

(Lee et al., 2005, 2009). We found that amputation at a proximal position results in a proximal shift of the *cyp26a1* expression domain (Fig. 3F,G). In return, *cyp26a1* expression shifted distally during the course of regeneration (Fig. 3E). Notably, also the distal limit of aligned preosteoblasts was always adjacent to the distal limit of *cyp26a1* expression (Fig. 3E-H), suggesting that *cyp26a1*-expressing cells spatially confine preosteoblasts also along the proximodistal axis.

Conclusions

During fin regeneration the ray-interray organization has to be faithfully re-established in order to rebuild an exact copy of the lost fin parts and to ensure proper function of the regenerated fin. Here, we show that disrespect of the ray-interray boundaries by preosteoblasts and other blastema cells in the nascent blastema has adverse consequences for subsequent fin patterning and may disrupt the whole regeneration process. Our findings support a model in which signals from RA-degrading niches established by Cyp26a1 in the basal epidermal layer ensure the appropriate initial alignment of preosteoblasts in the nascent blastema (Fig. 4) and compel blastema cells to respect ray-interray boundaries. Furthermore, during regenerative outgrowth, Cyp26a1 activity remains important to facilitate Shha-promoted proliferation in adjacent preosteoblasts (Fig. 4).

MATERIALS AND METHODS

Zebrafish husbandry, fin amputations, heat shock and drug treatment conditions

Zebrafish were raised under standard conditions at 27-28°C. Caudal fins of 3- to 18-month-old fish were amputated along the dorsoventral axis, intersecting the median rays halfway for normal cuts, at ~30% ray length for proximal cuts, at ~70% for distal cuts, within 1-2 segments distal to the first branching point for short cuts and within the third segment away for long cuts. Heat shocks were performed at 38°C for 1 h. Approximately 20 µl RA (all-trans RA, Sigma) or R115866 (Janssen Pharmaceutica) were intraperitoneally injected into size-matched siblings every 12 h. RA: 1 mM in 1% DMSO/PBS. R115866: 0.67 mM 10% DMSO/PBS. For cyclopamine treatment, fish were incubated in 5 µM cyclopamine (Sigma), 0.1% EtOH, 0.1% DMSO in E3-medium (HEPES-buffered at pH 7.4). Cyclopamine was exchanged daily. SAG (Calbiochem) treatment was performed using 5 µM SAG in E3-medium. SAG stock solution was prepared in water. Control fish were always treated with an equivalent concentration of the drug solvent. All animal experiments were approved by the state of Baden-Württemberg, Germany.

Osteoblast differentiation, qPCR, TUNEL staining, EdU labeling and cryosectioning

Osteoblast differentiation was examined by measuring the GFP-free distal region in *osx:gfp* fish (*Olsp7:nlsgfp*; Spoorendonk et al., 2008). Gene expression levels were analyzed by qPCR (for primers see supplementary material Table S1), cell death by TUNEL staining and cell proliferation by EdU labeling. Cryosectioning was used to produce longitudinal and transverse fin sections. Further information concerning these methods, as well as descriptions of length measurements and cell number quantifications, imaging, immunohistochemistry, *in situ* hybridization and Alizarin Red staining can be found in the supplementary material methods.

Statistics

Student's *t*-test was used to test significance of differences. The numbers of specimens used are given in supplementary material Table S2.

Acknowledgements

We thank S. Schulte-Merker, K. Poss and U. Strähle for transgenic fish lines, Janssen Pharmaceutica for the R115866 compound, and A. Pfeifer, I. Zerenner-Fritsche, S. Leuschner and K.-H. Pöhner for fish care.

Competing interests

The authors declare no competing or financial interests.

Author contributions

N.B. conceived the study, and designed, performed and analyzed experiments. N.B. and G.B. wrote the manuscript.

Funding

N.B. was supported by fellowships from the University of Konstanz and the Research Training Group (RTG) 1331, and by a travelling fellowship from The Company of Biologists. This work was supported by a grant from the Deutsche Forschungsgemeinschaft [BE 1902/6-1 to G.B.].

Supplementary material

Supplementary material available online at
http://dev.biologists.org/lookup/suppl/doi:10.1242/dev.120212/-/DC1

References

Akimenko, M. A., Johnson, S. L., Westerfield, M. and Ekker, M. (1995). Differential induction of four msx homeobox genes during fin development and regeneration in zebrafish. *Development* **121**, 347-357.

Akimenko, M.-A., Marí-Beffa, M., Becerra, J. and Géraudie, J. (2003). Old questions, new tools, and some answers to the mystery of fin regeneration. *Dev. Dyn.* **226**, 190-201.

Blum, N. and Begemann, G. (2012). Retinoic acid signaling controls the formation, proliferation and survival of the blastema during adult zebrafish fin regeneration. *Development* **139**, 107-116.

Blum, N. and Begemann, G. (2015). Osteoblast de- and redifferentiation are controlled by a dynamic response to retinoic acid during zebrafish fin regeneration. *Development* **142**, 2894-2903.

Ertzer, R., Müller, F., Hadzhiev, Y., Rathnam, S., Fischera, N., Rastegara, S. and Strähle, U. (2007). Cooperation of sonic hedgehog enhancers in midline expression. *Dev. Biol.* **301**, 578-589.

Ferretti, P. and Géraudie, J. (1995). Retinoic acid-induced cell death in the wound epidermis of regenerating zebrafish fins. *Dev. Dyn.* **202**, 271-283.

Gemberling, M., Bailey, T. J., Hyde, D. R. and Poss, K. D. (2013). The zebrafish as a model for complex tissue regeneration. *Trends Genet.* **29**, 611-620.

Géraudie, J. and Ferretti, P. (1997). Correlation between RA-induced apoptosis and patterning defects in regenerating fins and limbs. *Int. J. Dev. Biol.* **41**, 529-532.

Géraudie, J., Monnot, M. J., Brulfert, A. and Ferretti, P. (1995). Caudal fin regeneration in wild type and long-fin mutant zebrafish is affected by retinoic acid. *Int. J. Dev. Biol.* **39**, 373-381.

Hernandez, R. E., Putzke, A. P., Myers, J. P., Margaretha, L. and Moens, C. B. (2007). Cyp26 enzymes generate the retinoic acid response pattern necessary for hindbrain development. *Development* **134**, 177-187.

Huang, C.-c., Lawson, N. D., Weinstein, B. M. and Johnson, S. L. (2003). Reg6 is required for branching morphogenesis during blood vessel regeneration in zebrafish caudal fins. *Dev. Biol.* **264**, 263-274.

Knopf, F., Hammond, C., Chekuru, A., Kurth, T., Hans, S., Weber, C. W., Mahatma, G., Fisher, S., Brand, M., Schulte-Merker, S. et al. (2011). Bone regenerates via dedifferentiation of osteoblasts in the zebrafish fin. *Dev. Cell* **20**, 713-724.

Development (2015) 142, 2888-2893 doi:10.1242/dev.120212

Laforest, L., Brown, C. W., Poleo, G., Géraudie, J., Tada, M., Ekker, M. and Akimenko, M. A. (1998). Involvement of the sonic hedgehog, patched 1 and bmp2 genes in patterning of the zebrafish dermal fin rays. *Development* **125**, 4175-4184.

Lawson, N. D. and Weinstein, B. M. (2002). In vivo imaging of embryonic vascular development using transgenic zebrafish. *Dev. Biol.* **248**, 307-318.

Lee, Y., Grill, S., Sanchez, A., Murphy-Ryan, M. and Poss, K. D. (2005). Fgf signaling instructs position-dependent growth rate during zebrafish fin regeneration. *Development* **132**, 5173-5183.

Lee, Y., Hami, D., De Val, S., Kagermeier-Schenk, B., Wills, A. A., Black, B. L., Weidinger, G. and Poss, K. D. (2009). Maintenance of blastemal proliferation by functionally diverse epidermis in regenerating zebrafish fins. *Dev. Biol.* **331**, 270-280.

Quint, E., Smith, A., Avaron, F., Laforest, L., Miles, J., Gaffield, W. and Akimenko, M.-A. (2002). Bone patterning is altered in the regenerating zebrafish caudal fin after ectopic expression of sonic hedgehog and bmp2b or exposure to cyclopamine. *Proc. Natl. Acad. Sci. USA* **99**, 8713-8718.

Sousa, S., Afonso, N., Bensimon-Brito, A., Fonseca, M., Simões, M., Leon, J., Roehl, H., Cancela, M. L. and Jacinto, A. (2011). Differentiated skeletal cells contribute to blastema formation during zebrafish fin regeneration. *Development* **138**, 3897-3905.

Spoorendonk, K. M., Peterson-Maduro, J., Renn, J., Trowe, T., Kranenbarg, S., Winkler, C. and Schulte-Merker, S. (2008). Retinoic acid and Cyp26b1 are critical regulators of osteogenesis in the axial skeleton. *Development* **135**, 3765-3774.

Stewart, S. and Stankunas, K. (2012). Limited dedifferentiation provides replacement tissue during zebrafish fin regeneration. *Dev. Biol.* **365**, 339-349.

Stewart, S., Gomez, A. W., Armstrong, B. E., Henner, A. and Stankunas, K. (2014). Sequential and opposing activities of Wnt and BMP coordinate zebrafish bone regeneration. *Cell Rep.* **6**, 482-498.

Stoppie, P., Borgers, M., Borghgraef, P., Dillen, L., Goossens, J. A. N., Sanz, G., Szel, H., Hove, C. V. A. N., Nyen, G. V. A. N., Nobels, G. et al. (2000). R115866 inhibits all- trans -retinoic acid metabolism and exerts retinoidal effects in rodents. *J. Pharmacol. Exp. Ther.* **293**, 304-312.

Tanaka, E. M. and Reddien, P. W. (2011). The cellular basis for animal regeneration. *Dev. Cell* **21**, 172-185.

White, J. A., Boffa, M. B., Jones, B. and Petkovich, M. (1994). A zebrafish retinoic acid receptor expressed in the regenerating caudal fin. *Development* **120**, 1861-1872.

Zhang, J., Jeradi, S., Strähle, U. and Akimenko, M.-A. (2012). Laser ablation of the sonic hedgehog-a-expressing cells during fin regeneration affects ray branching morphogenesis. *Dev. Biol.* **365**, 424-433.

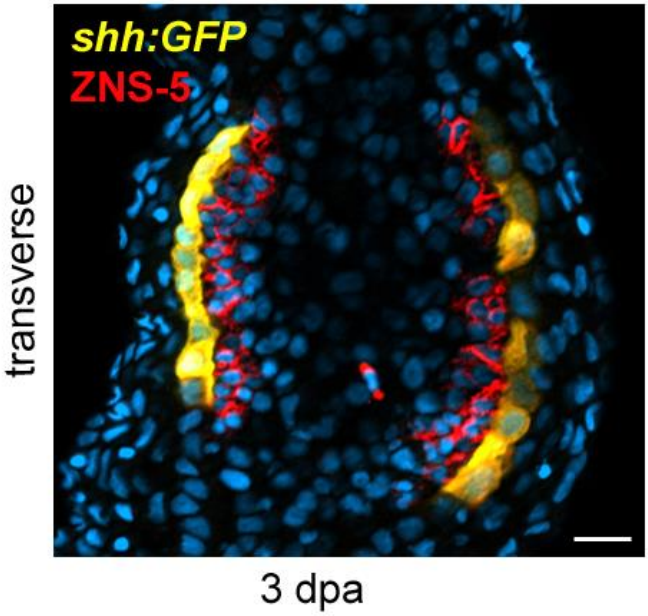

Fig. S1. *shha* is expressed within the basal epidermal layer adjacent to aligned osteoblasts.

IHC for ZNS-5 and GFP in *shh:gfp* fish at 3 dpa reveals *shha* expression in the basal epidermal layer adjacent to osteoblasts (ZNS-5^{+}). Scale bar: 50 µm.

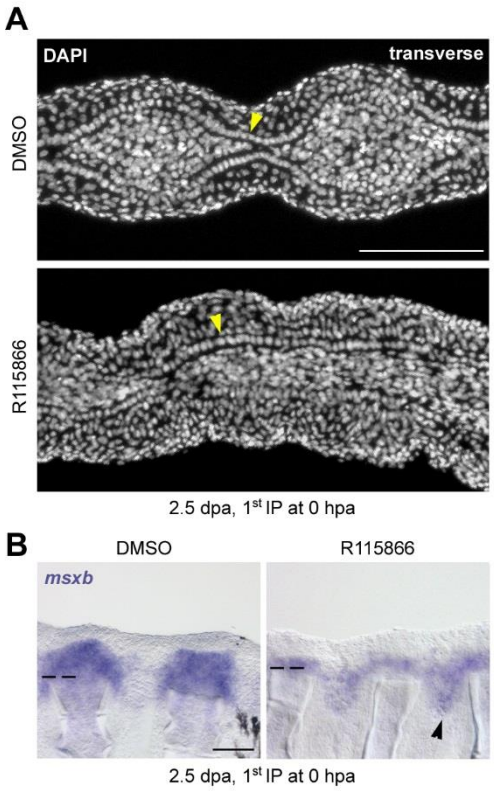

Fig. S2. R115866 treatment does not interfere with basal epidermal layer formation, but cause lateral expansion of *msxb*$^{+}$ cells into neighbouring interrays.

(A) DAPI-stained transverse sections through the regenerate of DMSO- and R115866-treated fish reveal presence of a distinct basal epidermal layer. Arrowheads: Basal epidermal layer. (B) WISH for *msxb* at 2.5 dpa demonstrates expansion of blastema cells into interrays in R115866-treated fish. Arrowheads: Ectopic blastema cells. Dashed lines indicate amputation plane. Scale bars: 50 µm in A and 100 µm in B.

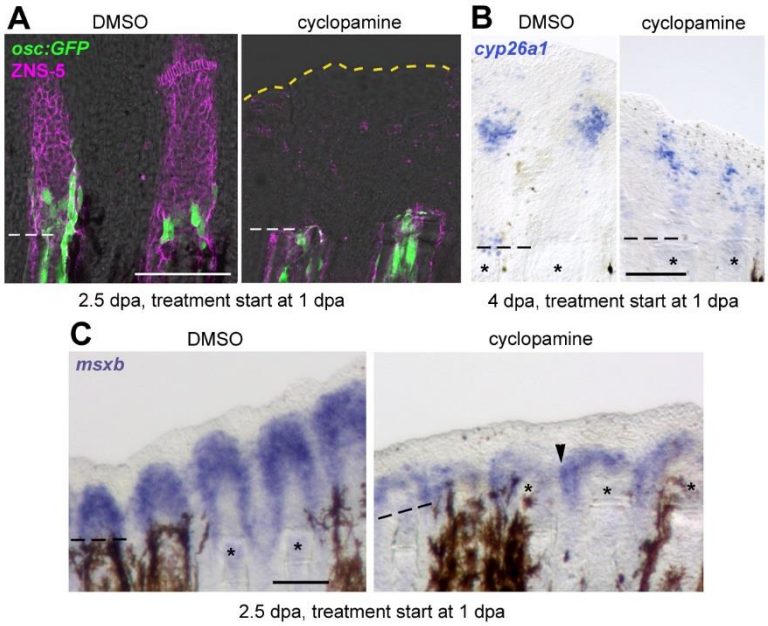

Fig. S3. Absence of preosteoblasts causes blastema expansion.

Cyclopamine treatment starting at 1 dpa results in preosteoblast-free blastema and lateral expansion of blastema cells, but normal *cyp26a1* expression. (A) IHC for ZNS-5 and GFP in *osc:gfp* fish demonstrates lack of GFP^+ preosteoblasts in the blastema of cyclopamine treated fish at 2.5 dpa. Yellow dashed line indicates the distal blastema edge in cyclopamine treated fish. (B) WISH for *cyp26a1* at 4 dpa reveals unaltered *cyp26a1* expression in cyclopamine treated fish (C) WISH for *msxb* demonstrates lateral expansion of blastema cells into the interray tissue (arrowhead) in cyclopamine treated fish. Dashed lines indicate amputation plane. Scale bars: 100 μm.

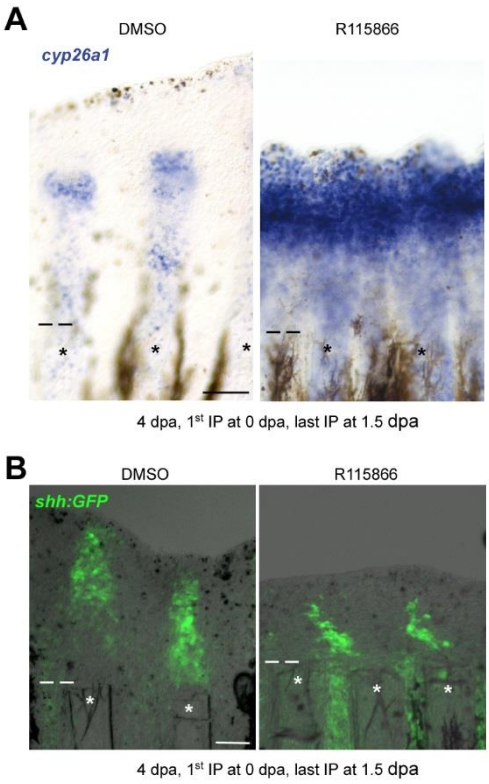

Fig. S4. *shha* expression is ectopically expressed in interrays upon recovery from R115866 treatment.

(A) WISH for *cyp26a1* 2 days after termination of R115866 treatment at 4 dpa reveals *cyp26a1* expression in the entire epidermis of ray and interray tissue. (B) IHC for GFP in *shh:gfp* fish 2 days after termination of R115866 treatment at 4 dpa reveals ectopic *shha* expression in interrays. Asterisks indicate rays. Dashed lines indicate amputation plane. Scale bars: 100 µm.

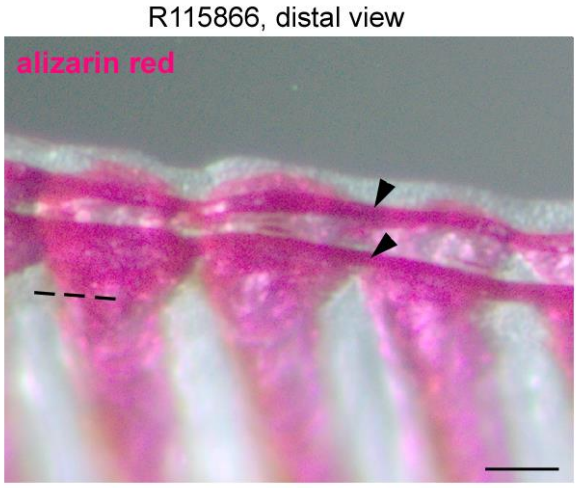

Fig. S5. Ectopic bone does not seal the wound in regenerates of R115966 treated fish.

Distal view of an Alizarin Red stained regenerate of R115866-treated fish reveals that ectopic bone is restricted to lateral regions and does not seal the blastema. Arrowheads: Ectopic bone in the interray region. Dashed line indicate amputation plane. Scale bars: 100 µm.

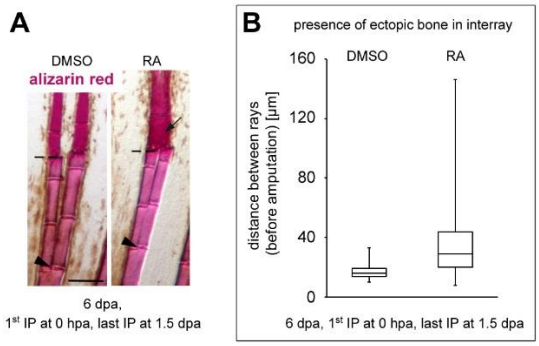

Fig. S6. RA treatment induces ectopic bone in interrays and fusion of sister rays.

(A) RA injections upon amputation within 3-4 segments distal to the first branching point (long cut) result in fusion of sister rays. Alizarin Red staining. Arrowheads: Branching site. Dashed lines indicate amputation plane. Scale bar: 100 µm. (B) The distance range between rays where formation of ectopic bone occurs is much greater in RA-treated fish. Box plot of distances between rays.

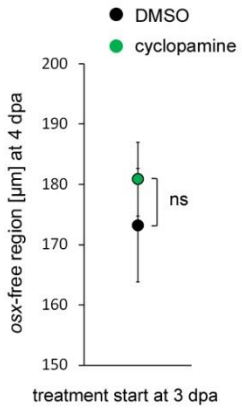

Fig. S7. Cyclopamine treatment does not impair osteoblast differentiation.

Length measurement of the *osx*-free distal domain (tissue that does not contain differentiated osteoblasts) in *osx:gfp* fish at 4 dpa reveals that the osteoblast differentiation is unaffected in cyclopamine-treated fish. Data are represented as mean±s.e.m. ns, non significant.

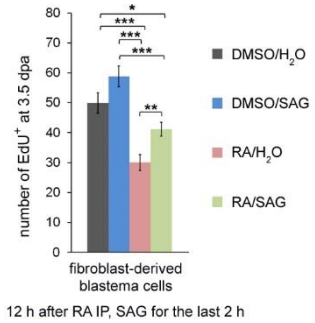

Fig. S8. Prolonged RA treatment impairs proliferation of fibroblast-derived blastemal cells through repression of Hh signaling.

Inhibition of proliferation of fibroblast-derived blastemal cells 12 h after RA injection can be rescued by concomitant SAG treatment. EdU^+ cells per section at 3.5 dpa. Data are represented as mean±s.e.m. *p < 0.05, **p < 0.01, ***p < 0.001.

Supplementary Materials and Methods

Zebrafish lines

Konstanz wild type, *Ola.bglap:egfp*^{hu4008} (Knopf et al., 2011), *Ola.sp7:nls-gfp*^{zf132} (Spoorendonk et al., 2008), *hsp70l:dnfgfr1-egfp*^{pd1} (Lee et al., 2005), *hsp70l:v-ras*^{pd9} (Lee et al., 2009), *2.2shh:gfp*:ABC#15^{sb15} (Ertzer et al., 2007) and *fli1a:egfp*^{y1} (Lawson and Weinstein, 2002) fish were used. Heat-shock lines were analyzed as heterozygotes; wild type siblings served as controls.

Examination of osteoblast differentiation

Because osteoblast differentiation is accompanied by upregulation of *osx*, we used *gfp* expression in *osx:gfp* fish (*Ola.sp7:nlsgfp*) as marker for differentiated osteoblasts and determined the length of the *osx*-free distal region to detect putative effects on osteoblast differentiation.

Length measurements and quantification of cell numbers

Length measurements were performed on the third dorsal and/or the third ventral fin ray. EdU- or TUNEL-labeled cells were counted in the tissue distal to the amputation plane in longitudinal sections. The distance between (sister) rays were measured at the amputation site.

qPCR analysis

Tissue distal to the amputation plane was used for RNA extraction. Tissues from 4-10 fish were pooled for each RNA sample. Trizol reagent (Invitrogen) or TriPure (Roche) was used for RNA extraction. RNA was treated with DNase I and equal amounts of total RNA from

each sample were reverse transcribed with SuperScript III reverse transcriptase (Invitrogen) or Maxima Reverse Transcriptase (Thermo Scientific) using anchored oligo(dT) primers. A C1000 thermal cycler combined with a CFX96 real-time PCR detection system (Bio-Rad) was used for quantitative real-time PCR (qPCR). PCR reactions were performed by using the Maxima SYBR Green qPCR Master Mix (Thermo Scientific). qPCR reactions for each cDNA pool and each target gene were performed in triplicates. Data were analyzed with the CFX Manager software (Bio-Rad). *ef1a*, *tbp* and *actb1* expression levels were used for normalization. Expression levels were normalized to expression levels of two reference genes (expression stability: Mean M <0.5) and expression ratios were calculated relative to control samples. Regenerates of heat-shocked non-transgenic siblings were used as control if expression levels were examined in *hsp70l:dn-fgfr1* or *hsp70l:v-ras* fish and regenerates of vehicle treated fish were used as control if expression levels were examined in RA- or R115866 treated fish. Reference genes were used in different combinations, depending on the treatment condition. If normalization to different reference genes gave conflicting results (expression stability: Mean M ≥0.5), results were verified by normalization to the input RNA amount by performing RiboGreen or Qubit assays (Invitrogen). Primers are listed in Table S1.

Imaging

Images were captured with the Zeiss AxioVision or Zeiss ZEN software on a Zeiss Stemi 2000-C stereomicroscope equipped with a AxioCam ERc5s, a Leica MZ10F stereomicroscope equipped with a AxioCam MRc or a Zeiss Axio Imager.M2 equipped with a AxioCam MRc or a AxioCam MRm. For fluorescent microscopy of IHC or EdU stained fins structured illumination microscopy was used (Zeiss ApoTome.2, Zeiss Axio Imager.M2). Zeiss ZEN and Adobe Photoshop were used for image processing and length measurements.

Cryosectioning

Fixed (and stained) fins were decalcified in 10 mM EDTA in PBT (PBS containing 0.1% Tween20), embedded in 1.5% agar, 5% sucrose in PBS and soaked in 30% sucrose in PBS. Embedded fins were snap-frozen in Tissue-Tek O.C.T. Compound (Sakura) in liquid nitrogen and sections were cut at 16 µm.

Immunohistochemistry

For IHC, fins were fixed in 4% Paraformaldehyde (PFA) in PBS and stored in MeOH at –20°C. IHC was performed on cryosections or whole mounts. Sections or fins were permeabilized in PBTx (PBS containing 0.3% Triton X-100) (30 min for sections and 1 hour for whole mounts), blocked in 2% blocking reagent (Roche) in PBT and subsequently incubated with primary antibodies over night at 4°C. Tissue was washed and incubated with secondary antibodies for 3-4 hours at room temperature or over night at 4°C. Whole mounts were transferred to 70% glycerol in PBS for imaging. Sections were counterstained with DAPI and mounted using Mowiol containing DABCO. The following antibodies and dilutions were used: mouse ZNS-5 (an uncharacterized cell surface antigen that is specifically present on osteoblasts irrespective of their differentiation status) (Zebrafish International Resource Center) 1:1500, rabbit anti-GFP (Invitrogen, A6455) 1:500. Alexa Fluor®- (Invitrogen), Atto- (Sigma) or alkaline phosphatase (AP) - (Sigma) conjugated secondary antibodies were used. NBT/BCIP (Roche) was used as substrate for alkaline phosphatase.

TUNEL labeling

TUNEL labeling was performed in combination with IHC for ZNS-5 on cryosections. Fins were fixed in 4% PFA and stored in MeOH at –20°C. Sections were permeabilized for 30 min in PBTx and equilibrated in terminal deoxynucleotidyl transferase (TdT) buffer (200 mM

potassium cacodylate, 25 mM Tris, 0.05% Triton X-100, 1 mM CoCl2, pH 7.2). Subsequently sections were incubated with TdT buffer containing 0.5 µM fluorescein-12-dUTP, 40 µM dTTP and 0.02 units/µl TdT (all Thermo Scientific) for 1-2 hours at 37°C. Sections were washed in PBT, blocked in 2% Blocking Reagent in PBS and incubated with anti-fluorescein-alkaline phosphatase coupled antibody (1:2000, Roche) and ZNS-5 antibody (1:1500) at 4°C over night. TUNEL labeled cells were detected with NBT/BCIP, AP activity was quenched with 100 mM glycin (pH 2.2) and ZNS-5 labeled cells were detected with anti-mouse-AP-coupled antibody (Sigma) using INT/BCIP (Roche) as substrate. Sections were mounted using Mowiol.

EdU labeling

Fish were IP injected with approximately 20 µl of 2.5 mg EdU (Jena Bioscience) in PBS 30 minutes prior to fixation. Fins were fixed in 4% PFA and stored in MeOH at –20°C. EdU labeling was performed on whole mounts and cryosectioning was performed afterwards. For EdU detection, fins were permeabilized in PBTx for 30 min, equilibrated in 100 mM Tris/HCl pH 8 and EdU was detected using a copper-catalyzed azide-alkyne click chemistry reaction (0.6 µM Cy3- or Fluor488- labeled azides (Jena Bioscience), 100 mM Tris, 1 mM CuSO4, 100 mM ascorbic acid, pH 8) with 20 min incubation time. IHC for ZNS-5 was subsequently performed on sections. Sections were counterstained with DAPI and mounted using Mowiol containing DABCO. Whole mounts were transferred to 70% glycerol/PBS for imaging.

In situ hybridization

Digoxigenin labeled RNA antisense probes were synthesized from cDNA templates: *aldh1a2* (Grandel et al., 2002), *cyp26a1* (Kudoh et al., 2002), *msxb* (Akimenko et al., 1995), *shha* (Quint et al., 2002). WISH and ISH on sections was performed as previously described (Blum and Begemann, 2012). For double WISH DIG- and fluorescein-labeled probes were

hybridized simultaneously. Fins were first incubated with anti-DIG-AP coupled antibody and color reaction was performed with BCIP/NBT. AP activity was quenched with 100 mM glycin (pH 2.2) and fluorescein was detected by using anti-fluorescein-AP coupled antibody and INT/BCIP as substrate.

Alizarin Red staining

For Alizarin Red staining, fins were fixed in 4% PFA in PBS, transferred to MeOH and stored at -20°C. Fins were rehydrated, washed in PBT and stained in 0.1% Alizarin Red in 0.5% KOH overnight. Excess dye was removed by several washes in 0.5% KOH. Stained fins were transferred to 70% glycerol in 0.5% KOH for imaging.

Supplementary References

Grandel, H., Lun, K., Rauch, G.-J., Rhinn, M., Piotrowski, T., Houart, C., Sordino, P., Küchler, A. M., Schulte-Merker, S., Geisler, R., et al. (2002). Retinoic acid signalling in the zebrafish embryo is necessary during pre-segmentation stages to pattern the anterior-posterior axis of the CNS and to induce a pectoral fin bud. *Development* **129**, 2851–65.

Kudoh, T., Wilson, S. W. and Dawid, I. B. (2002). Distinct roles for Fgf, Wnt and retinoic acid in posteriorizing the neural ectoderm. *Development* **129**, 4335–46.

Table S1. Primer sequences for qPCR experiments.

Gene	Forward primer	Reverse primer
bactin1	TTGCTCCTTCCACCATGAAG	CTTGCTTGCTGATCCACATC
cyp26a1	GATGGGAGCTGATAATGTG	CCTGAACCTCCTCTCTGACC
ef1a	TACGCCTGGGTGTTGGACAAA	TCTTCTTGATGTATCCGCTGAC
ptch2	GGAGATTTACCCCCAAGTTAC	CCAACAGACAGGGCTCCG
shha	CGGCAGAAGAAGACATCC	GAGCAATGAATGTGGGCTTT
tbp	CGGTGGATCCTGCGAATTA	TGACAGGTTATGAAGCAAAACAACA

Table S2A. Number of specimens used in quantitative and nonquantitative experiments (Fig. 1-3). Numbers for corresponding experiments, which are not shown in the figure, are included. For nonquantitative experiments: the first number indicates the number of specimens showing the phenotype, the second number the total number.

Figure	n =
1C	36/39 rays (5 fins)
1D	fused rays = 37, separated rays = 138
1E	19/25 rays (10 fins)
1H	3 cDNA pools per condition
1I	DMSO = 0/5 fins, R115866 = 5/5 fins
1J,K	wild type = 0/11 fins, *hsp70l:cyp26a1* = 10/10 fins
1L	10/10 rays (4 fins)
2A	RA: DMSO = 0/30 fins, RA 30/31 fins; R115866: DMSO = 0/8 fins, R115866 = 9/9 fins
2B	DMSO = 0/23 fins, RA 21/21 fins
2C	DMSO = 0/8 fins, RA 9/9 fins
2D	RA: DMSO = 0/6 fins, RA 6/6 fins; R115866: DMSO = 0/6 fins, R115866 = 6/6 fins
2E	DMSO = 0/15 fins, R115866 19/19 fins
2F	DMSO = 0/21 fins, RA 4/22 fins
3A	DMSO = 20 sections (4 fins), cyclopamine = 35 sections (5 fins)
3B	DMSO = 22 sections (4 fins), RA = 24 sections (4 fins)
3C	24 sections (6 fins) per condition
3D	3 cDNA pools per condition
3E	*cyp26a1*: 3 dpa = 11 rays, 4 dpa = 6 rays, 5 dpa = 5 rays; ZNS-5: 3 dpa = 6 rays, 4 dpa = 9 rays, 5 dpa = 9 rays
3F	*cyp26a1*: proximal = 5 rays, distal = 5 rays; ZNS-5: proximal = 6 rays, distal = 7 rays

Table S2B. Number of specimens used in quantitative and nonquantitative experiments (Fig. S1-8). Numbers for corresponding experiments, which are not shown in the figure, are included. For nonquantitative experiments: the first number indicates the number of specimens showing the phenotype, the second number the total number.

Figure	n =
S2A	RA: DMSO = 5/5 fins, RA = 5/5 fins; R115866: DMSO = 6/6 fins, R115866 = 5/5 fins
S2B	DMSO = 0/12 fins, R115866 = 12/12 fins
S3A	DMSO = 0/8 fins, cylopamine = 9/9 fins
S3B	DMSO = 4/4 fins, cylopamine = 4/5 fins
S3C	DMSO = 0/10 fins, cylopamine = 11/11 fins
S4A	DMSO = 0/5 fins, R115866 = 4/4 fins
S4B	DMSO = 0/5 fins, R115866 = 5/6 fins
S6A	DMSO = 3/17 rays (5 fins), RA = 15/18 rays (6 fins)
S6B	DMSO = 32 rays, RA = 150 rays
S7	DMSO = 10 rays, cyclopamine = 12 rays
S8	24 sections (6 fins) per condition